ISSN 1070-3284, Russian Journal of Coordination Chemistry, 2016, Vol. 42, No. 10, pp. 662–678. © Pleiades Publishing, Ltd., 2016.
Original Russian Text © D.M. Tsymbarenko, I.A. Martynova, I.P. Malkerova, A.S. Alikhanyan, N.P. Kuzmina, 2016, published in Koordinatsionnaya Khimiya, 2016, Vol. 42, No. 10, pp. 624–639.

Mixed Ligand Acetate, Propionate, and Pivalate Complexes of Rare Earth Metals with Monoethanolamine: A New Approach to the Synthesis, Composition, Structure, and Use for the Preparation of Oxide Materials

D. M. Tsymbarenko[a], *, I. A. Martynova[a], I. P. Malkerova[b], A. S. Alikhanyan[b], and N. P. Kuzmina[a]

[a] *Moscow State University, Moscow, 119991 Russia*

[b] *Kurnakov Institute of General and Inorganic Chemistry, Russian Academy of Sciences, Leninskii pr. 31, Moscow, 119991 Russia*

**e-mail: tsymbarenko@gmail.com*

Received April 16, 2016

Abstract—Compositions of mixed ligand acetate, propionate, and pivalate complexes of rare earth metals of the cerium and yttrium groups with monoethanolamine are predetermined by the synthesis conditions and the nature of the carboxylate ligand and rare earth metal ion. Solid mixed ligand complexes $[Ln(Piv)_5(MEAH)][MEAH]$ and $[Ln(Piv)_3(MEA)]$, homoligand complexes $[Ln(Piv)_3]$ (HPiv is 2,2-dimethylpropionic (pivalic) acid), and gel-like hydroxo complexes $[Ln(Carb)_{3-x-y}(NO_3)_x(OH)_y(MEA)_w(H_2O)_z]$ (HCarb is acetic (HAc) or propionic (HProp) acid) are isolated using original synthesis procedures involving ion pairs $[MEAH]^+[Carb]^-$ (MEA is monoethanolamine). The compounds are studied by IR spectroscopy, ^1H NMR spectroscopy, elemental and thermal analyses, and mass spectrometry. Specific features for the complex formation of rare earth metal pivalates with MEA are additionally studied using quantum-chemical simulation.

Keywords: rare earth elements, carboxylates, mixed ligand complexes, metal-organic precursors, synthesis, mass-spectrometry, quantum-chemistry calculations

DOI: 10.1134/S1070328416100043

INTRODUCTION

The development of the coordination chemistry of rare earth metals in recent years is mainly due to the use of coordination compounds for the solution of problems of synthesis of new functional materials containing rare earth metals and for the development of new methods for their preparation. Among these materials, coatings based on rare earth metal oxides are of interest, since they find wide use in electronics, power engineering, electrical engineering, optics, nanotechnologies, etc. due to their unique properties [1].

One of the promising methods for the preparation of thin film functional materials based on rare earth metal oxides is the metal organic chemical solution deposition (MOCSD) method [2]. Metal-organic precursors (MOP) represent solutions of coordination compounds or salts of rare earth metals, and the formation of an oxide layer is described by the following sequence of physicochemical transformations:

$$MOP_{solution} \rightarrow MOP_{film} \rightarrow \text{thin film of rare earth metal oxide} + \text{gaseous products.}$$

The quality of the produced oxide coating (homogeneity/uniformity, no residual carbon) is mainly determined by the composition of the MOP and their properties. Metal-organic precursors should be homogeneous solutions and form continuous gel-like films decomposing to oxides at low temperatures (<700°C).

Rare earth metal carboxylates, viz., derivatives of aliphatic carboxylic acids RCOOH (HCarb), where R is proton or alkyl radical C_nH_{2n+1} with a low number of carbon atoms (n = 1–5), are widely used as MOP. On the one hand, a small hydrocarbon radical diminishes a risk of oxide film contamination with carbon. On the other hand, an increase in the length and degree of branching of the radical even in such a narrow group of acids favors an increase in the solubility of rare earth metal carboxylates in organic solvents, which is

important for prospects of their use in the MOCSD method.

Lower rare earth metal carboxylates (n = 1–5) are rather well studied from the point of view of both thermal stability [3–7] and crystal structure [7–15]. The rare earth metal carboxylates decompose to oxides in a range of 600–800°C [3–7]. Thermal stability decreases on going from acetates and pivalates with branching of the hydrocarbon radical [7].

It is known that acetates, propionates, butyrates, and pivalates crystallize as hydrates or adducts with the corresponding HCarb having a polymer or binuclear structural motif [8–15], which predetermines their low solubility in organic solvents. The solubility and thermal stability of rare earth metal carboxylates can be modified, for example, by the introduction of neutral N- and/or O-donor ligands into the coordination sphere of $Ln(Carb)_3$, i.e., due to the formation of mixed ligand complexes. It seems reasonable to study the formation of mixed ligand complexes with organic additives, which are often used in the MOCSD method to improve the film-forming properties of MOP (viscosity, sol–gel stabilization, wettability, and adhesion).

2-Ethanolamines (monoethanolamine, diethanolamine) and *N*,*N*′-ethylenediamines (ethylenediamine, diethylenetriamine) are widely used as such additives. These are weak bases comparable in strength with an aqueous solution of ammonia ($pK_b \approx 4.75$) and containing N,O- or N,N-donor atoms. Monoethanolamine (MEA, $NH_2CH_2CH_2OH$) is especially interesting among these amino compounds as the first representative of the 2-ethanolamine series. There are almost no published data on coordination compounds of rare earth metals with MEA. Only rare earth metal aminoethylates obtained from their isopropylates and MEA under anhydrous conditions were described [16]. According to these data, the nitrogen atom of MEA does not participate in coordination. In the coordination compounds of 3*d* elements, MEA acts as an O,N-donor ligand in neutral or deprotonated forms [17–19].

We successfully used MEA as a sol-forming agent in MOP based on acetates for the preparation of thin biaxially textured CeO_2 films by the MOCSD method [20]. The reaction of Ce^{3+} acetate with MEA affords mixed ligand hydroxo complexes of Ce^{4+} with MEA.

It seems interesting to study specific features of rare earth metal carboxylates with MEA for both the coordination chemistry of rare earth metals and materials science. The understanding of processes that occur in the course of preparing the MOP makes it possible to control the quality of the functional material already at the stage of precursor synthesis.

In this work, we chose acetates, propionates, and pivalates of rare earth metals of the cerium and yttrium groups as objects of the study. The choice of acetic (HAc), propionic (HProp), and pivalic (HPiv) acids is due to the fact that these are weak acids with almost equal values of pK_a (~5) but with different alkyl groups. Our interest in mixed ligand complexes of the chosen carboxylates with MEA as potential MOP resulted in the situation where we rejected to use absolute solvents and dry atmosphere in order to make the further processes of synthesis and use of MOP technologically simpler.

The influence of various factors (thermodynamic stability of rare earth metal carboxylates and mixed ligand complexes, affinity of the rare earth ion to hydrolysis, and solubility) on the compositions, properties, and structures of the formed products of the reactions of the chosen rare earth metal carboxylates with MEA was analyzed using our earlier published and new experimental data and theoretical simulation results.

SYNTHESIS AND CHARACTERIZATION OF MIXED LIGAND COMPLEXES OF RARE EARTH METAL ACETATES, PROPIONATES, AND PIVALATES WITH MEA

The possibility of forming mixed ligand complexes between rare earth metal carboxylates and MEA was checked for lanthanum, cerium(III), and europium(III) acetates and pivalates [21]. The mixed ligand complexes were synthesized by the reactions of hydrates $Ln(Carb)_3 \cdot nH_2O$ or adducts $Ln(Carb)_3(HCarb)_m$ with MEA excess in non-absolute organic solvents. The differences between acetates and pivalates were revealed during these syntheses. For example, in the syntheses with rare earth metal pivalates, solid mixed ligand complexes $[Ln(Piv)_3(MEA)]$ (Ln = La, Ce, and Eu) were formed, whereas gel-like mixed ligand hydroxo complexes $[Ln(Ac)_{n-y}(OH)_y(MEA)_w(H_2O)_z]$ (n = 3, Ln = La, Eu; n = 4, Ln = Ce) were formed in the case of acetates. Cerium in hydroxoacetate was oxidized from +3 to +4, whereas the oxidation state of cerium remained unchanged in the mixed ligand complex $[Ce(Piv)_3(MEA)]$. In addition, crystals of the accompanying cerium(III) complex $[Ce(Piv)_5(MEAH)][MEAH]$ were isolated in the course of the synthesis of the mixed ligand complex $[Ce(Piv)_3(MEA)]$. According to the X-ray diffraction data, the isolated complex is mononuclear, which is not frequent for rare earth metal carboxylates [22]. The observed differences are due to a higher resistance of rare earth metal pivalates to

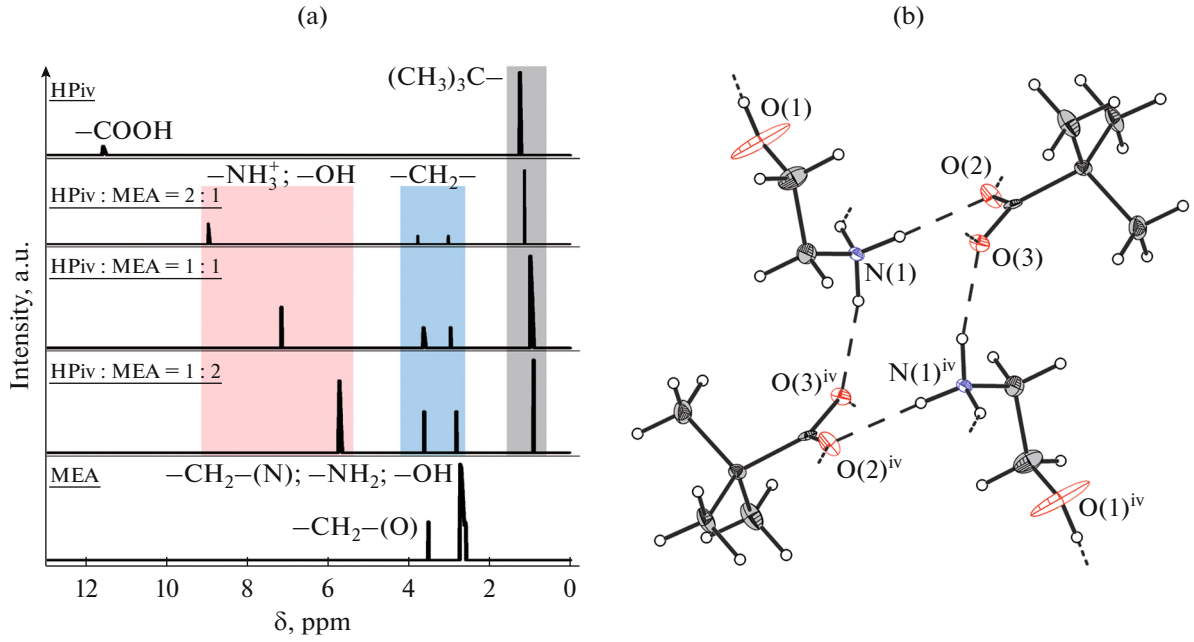

Fig. 1. Characterization of ion pairs in solution and in the crystalline state: (a) ^{1}H NMR spectra of HPiv–MEA solutions and (b) the dimeric fragment of the crystal structure of $[MEAH]^+[Piv]^-$.

hydrolysis under the action of MEA compared to acetates.

It is known that MEA binds organic acids into ion pairs $[HOCH_2CH_2NH_3]^+[Carb]^-$ [23, 24], whose formation neutralizes the alkaline properties of MEA, i.e., suppresses its hydrolyzing ability. This allowed us to propose a new approach to the synthesis of mixed ligand complexes of rare earth metals with MEA. The corresponding ion pairs $[MEAH]^+[Carb]^-$ were proposed to be used as a single source of carboxylate ions and MEA in non-absolute organic solvents.

Specific features of the formation and behavior of the ion pairs $[MEAH]^+[Carb]^-$ (HCarb = HAc, HProp, and HPiv) were studied by electrospray ionization mass spectrometry (ESI-MS) and ^{1}H NMR spectroscopy. The character of the ESI-MS spectra indicates that ion pairs $[MEAH]^+[Carb]^-$ and their adducts with HCarb or MEA are formed in solutions. No substantial changes in the character of the spectra were observed in the series of the chosen carboxylic acids. The comparative analysis of the ^{1}H NMR spectra of solutions of MEA–HPiv, HPiv, and MEA in $CDCl_3$ (Fig. 1a) suggested that the $[MEAH]^+[Piv]^-$ ion pair exists in the solution. In the spectra of $[MEAH]^+[Piv]^-$, the resonance signals of the protons of the COOH group in a range of 10.0–12.0 ppm are absent, whereas the resonance signals of the *tert*-butyl group are shifted by 0.1–0.2 ppm, indicating the deprotonation of HPiv. The resonance signals of the protons of the methylene groups of MEA at 2.5–4.0 ppm are split and shifted (by ~0.03 ppm), whereas the resonance signals of the protons of the OH and NH_2 groups are shifted to a range of 5.9–9.0 ppm, including due to the protonation of the NH_2 group. The ratios of integral intensities of the protons belonging to $MEAH^+$ and Piv^- correspond to the formation of the ion pair $[MEAH]^+[Piv]^-$ and its adducts $[MEAH]^+[Piv]^-(MEA)$ and $[MEAH]^+[Piv]^-(HPiv)$ at the initial molar ratios of the reactants 2 : 1 and 1 : 2, respectively.

Precipitates or gel phases are formed in solutions of MEA–HAc and MEA–HProp in $CDCl_3$ and CD_3CN, which impeded a correct ^{1}H NMR analysis, but the general character of changing the spectra does not differ from that for pivalic acid. All the data obtained showed the presence of the ion pairs $[MEAH]^+[Carb]^-$ and their adducts in all studied non-aqueous solutions. Crystalline salt $[MEAH]^+[Piv]^-$ of the layered structure was isolated. The layers consist of centrosymmetric dimeric fragments $[[MEAH]^+[Piv]^-]_2$ (Fig. 1b). All hydrogen atoms of the OH and NH_3^+ groups in the $MEAH^+$ cation form hydrogen bonds with the oxygen atoms of the Piv^- anions (D···A = 2.786(4), 2.759(3), 2.760(3), and 2.693(12) Å for the interactions N(1)–H(1)···O(2)^{iii}, N(1)–H(2)···O(3)^{iv}, N(1)–H(3)···O(2), and O(1)–H(4)···O(3)^{v}, respectively).

The approach proposed for the synthesis of mixed ligand complexes using ion pairs was tested in the reactions of hydrated lanthanum and lutetium nitrates with solutions of $[MEAH]^+[Carb]^-$ (HCarb = HAc, HProp, and HPiv) in organic solvents (Scheme 1, reaction (1a)). The molar ratio of the reactants equal to 1 : 5 was chosen in such a way that the binding of nitrate ions into $[MEAH]^+[NO_3]^-$ and the formation of mixed ligand complexes of carboxylates with MEA would be provided. The products were identified by the data of elemental analysis, IR spectroscopy, and ^1H NMR. The syntheses via reaction (1a) afforded gel-like and crystalline mixed ligand complexes for the interactions of rare earth metal acetates and pivalates with MEA [21]. The reactions with $[MEAH]^+[Carb]^-$ (HCarb = HAc and HProp) gave gel-like mixed ligand hydroxo complexes $[Ln(Carb)_{3-x-y}(NO_3)_x(OH)_y(MEA)_w(H_2O)_z]$ (Ln = La and Lu), and the reactions with $[MEAH]^+[Piv]^-$ afforded solid products $[La(Piv)_3MEA]$ and $[Lu(Piv)_3]$. The formation of a precipitate of $[Lu(Piv)_3]$ (Scheme 1, reaction (1a)) instead of a mixed ligand complex with MEA can be due to a very low solubility of $[Lu(Piv)_3]$ in organic solvents [25].

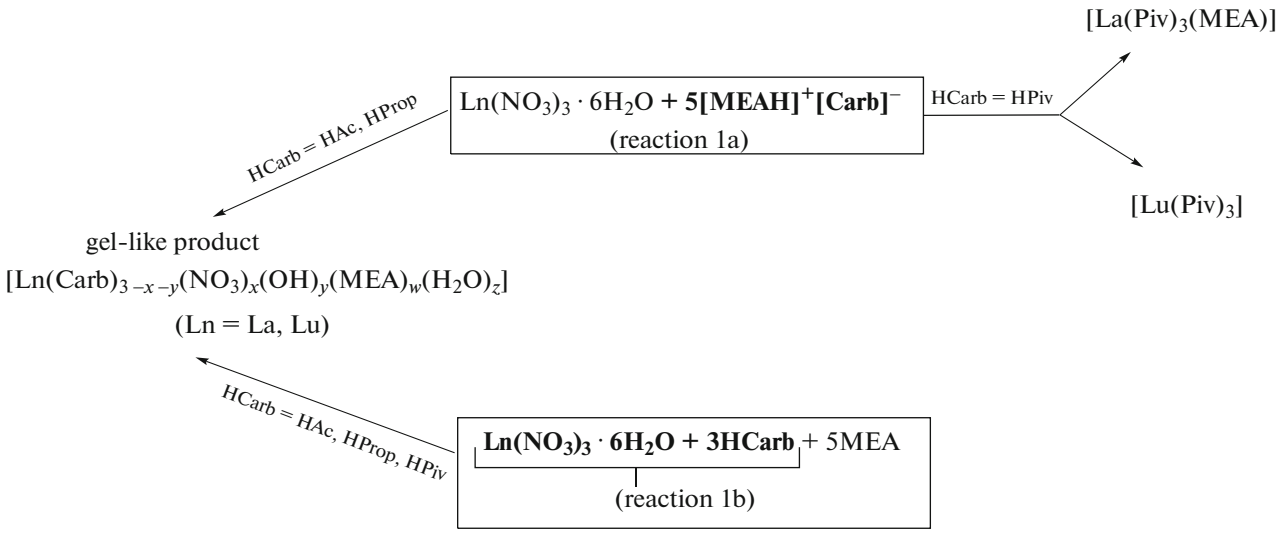

Scheme 1.

The role of the ion pair $[MEAH]^+[Piv]^-$ in the suppression of hydrolysis was demonstrated in the syntheses via reaction (1b) in Scheme 1. Monoethanolamine was added to a mixture of rare earth metal nitrate and carboxylic acid in the molar ratio $Ln(NO_3)_3$: HCarb : MEA = 1 : 3 : 5. Rare earth metal nitrates and carboxylic acids almost do not interact with each other, while the addition of MEA induces the parallel occurrence of the hydrolysis of hydrated nitrates, deprotonation of HCarb, and formation of mixed ligand hydroxogels for acetic, propionic, and pivalic acids (Scheme 1). It should be mentioned that in [26] reaction (1b) afforded the mixed ligand complexes $[Ln_2(MDEA)_2(Piv)_6]$ (Ln = La, Ce, Pr, Nd, and Sm; MDEA is *N*-methyldiethanolamine). Hydrolysis did not occur because of a lower basicity of MDEA as a tertiary amine with bulky substituents [27].

Thus, in the series of the studied ion pairs $[MEAH]^+[Carb]^-$, the hydrolysis is suppressed completely only in the case of $[MEAH]^+[Piv]^-$ in the reactions with hydrated rare earth metal nitrates (Scheme 1). This behavior is most probably related to an increase in the thermodynamic stability of $Ln(Carb)_3$ with the elongation and branching of the hydrocarbon radical in the series $Ac^- < Prop^- < Piv^-$ [28], especially in non-aqueous solvents [29].

The influence of the rare earth metal nature on the formation of mixed ligand complexes was studied for the reactions of rare earth metal pivalates and hydrated nitrates (Ln = La, Ce, Eu, Gd, Tb, Dy, Er, Tm, Yb, Lu, and Y) the with ion pair $[MEAH]^+[Piv]^-$ in acetonitrile via reactions (1a) and (2) (Scheme 2).

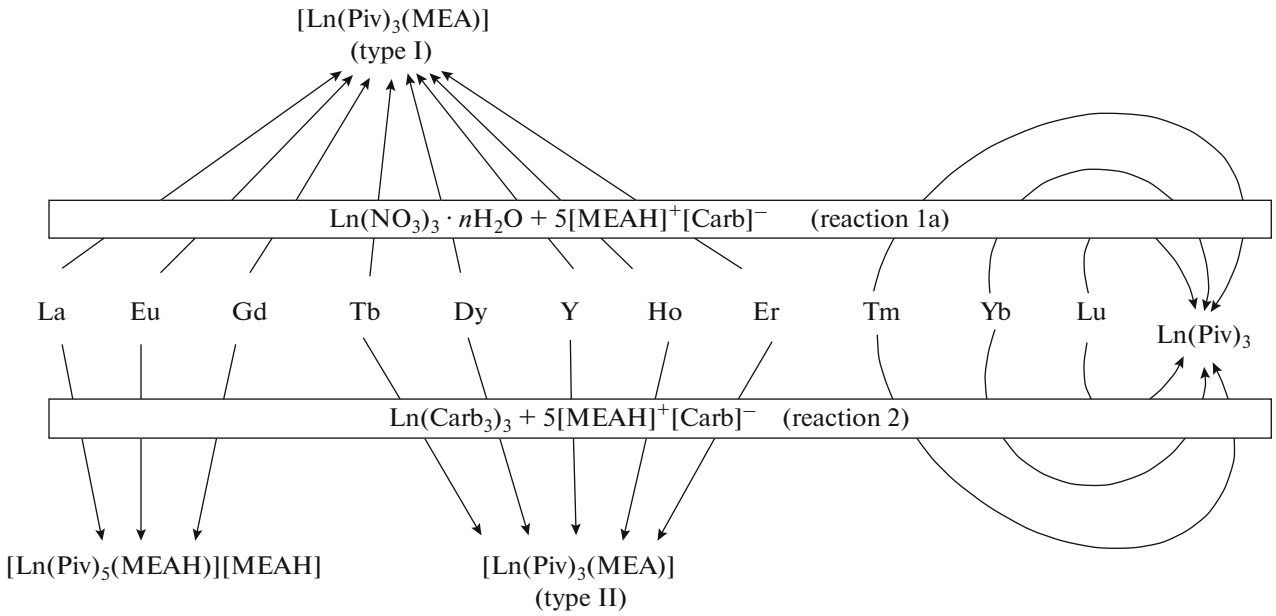

Scheme 2.

In the La–Er raw, including Y, reaction (1a) afforded mixed ligand complexes $[Ln(Piv)_3(MEA)]$, which are isostructural to each other according to the X-ray diffraction data (structural type **I**).

The reaction of $Ln(Piv)_3$ with $[MEAH]^+[Piv]^-$ excess (Scheme 2, reaction (2)) results in the formation of three groups of compounds: $[Ln(Piv)_5(MEAH)][MEAH]$ (Ln = La–Gd), $[Ln(Piv)_3(MEA)]$ (structural type **II**, Ln = Tb–Er, Y), and $[Ln(Piv)_3]$ (Ln = Tm–Lu). All complexes $[Ln(Piv)_5(MEAH)][MEAH]$ are isostructural (see Experimental), as well as $[Ce(Piv)_5(MEAH)][MEAH]$ for which X-ray diffraction analysis was carried out [22].

Mixed ligand complex $[Ce(Piv)_5(MEAH)][MEAH]$ is unique in structure, which is different from the known carboxylate compounds of rare earth metals (Fig. 2). The crystal structure of $[Ce(Piv)_5(MEAH)][MEAH]$ consists of mononuclear complex anions $[Ce(Piv)_5(MEAH^+)]^-$ and cations $[MEAH]^+$ joined by hydrogen bonds into layers between which only van der Waals interactions are observed. The central cerium ion in the anion coordinates six oxygen atoms of three bidentate chelate anions Piv^-, two oxygen atoms of two monodentate anions Piv^-, and the O(12) atom of the monoethanolamine molecule existing in the aminoprotonated cationic form. The coordination geometry of cerium can be described as a three-capped trigonal prism.

Mixed ligand complexes $[Ln(Piv)_3(MEA)]$ (Ln = Tb–Er) crystallize in two structural types (types **I** and **II**, Scheme 2) depending on the synthesis procedure, which can be due to the existence of several modifications of the mixed ligand complexes $[Ln(Piv)_3(MEA)]$. It is most likely that compounds $[Ln(Piv)_3(MEA)]$ have a polymer structure similar to $[Ba(Tfa)_2MEA]$ [30] and determined by the initial reactants or their molar ratios. The influence of the molar ratio of reactants on the composition of the formed coordination compounds was additionally studied for lanthanum and erbium. For example, reaction (1a) (Scheme 2) with the changed molar ratio equal to 1 : 3 produces a crystalline precipitate of $[Er(Piv)_3]$, and the mixed ligand complex $[Er(Piv)_3(MEA)]$ is formed at a ratio of 1 : 5. A decrease in the molar fraction of the ion pair from 5 to 3 in reaction (2) (Ln = La, Scheme 2) results in the formation of complex $[La(Piv)_3(MEA)]$ instead of $[La(Piv)_5(MEAH)][MEAH]$.

In the case of heavy rare earth metals (Ln = Tm–Lu), all microcrystalline precipitates obtained by reactions (1a) and (2) are anhydrous and non-solvated rare earth metal pivalates isostructural to each other and to $[Tm(Piv)_3]$ described earlier [31].

A change in the composition of the mixed ligand complexes in the raw of rare earth metals can be explained by an increase in the stability of pivalates and a decrease in the ionic radius. The elements of the beginning of REE raw are characterized by large ionic radii and high coordination numbers providing mixed ligand complexes with five pivalates anions, one O-coordinated $MEAH^+$, and one outer-sphere $MEAH^+$. Complexes $[Ln(Piv)_5(MEAH)][MEAH]$ were synthesized only via reaction (2) and only for large Ln = La–Gd. In the raw of rare earth metals, the composition of the mixed ligand complexes with piv-

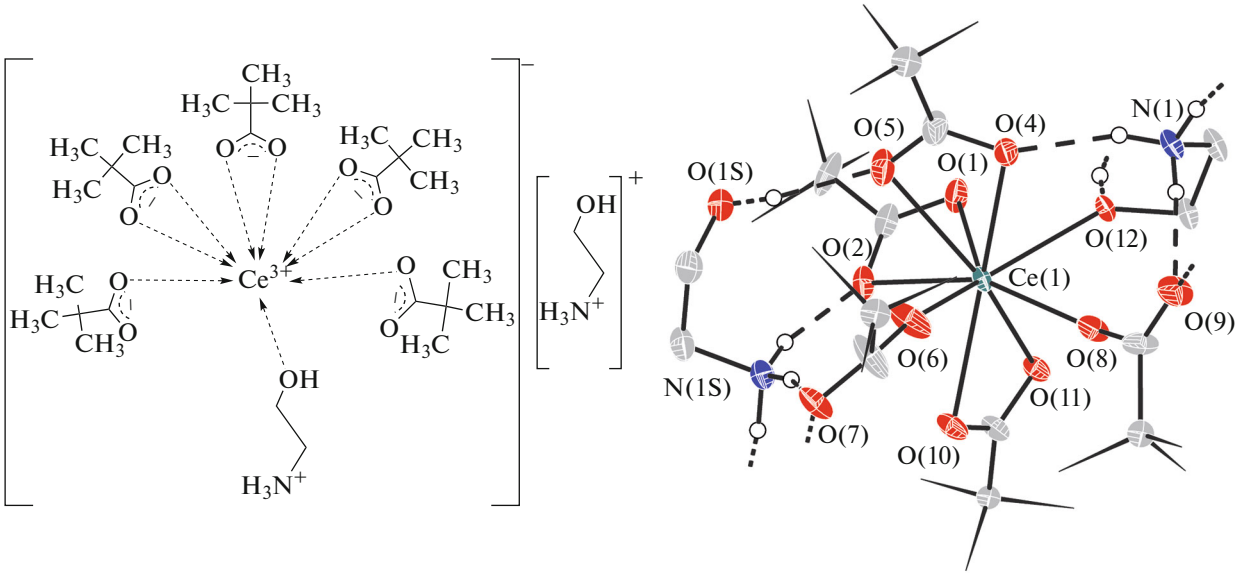

Fig. 2. Scheme and the structure of molecule $[Ce(Piv)_5(MEAH)][MEAH]$ [22] (some hydrogen atoms are omitted, and *tert*-butyl groups are shown schematically).

alate ligands and MEA changes from the mononuclear complexes $[Ln(Piv)_5(MEAH)][MEAH]$ (beginning of REE raw) to polymer complexes $[Ln(Piv)_3(MEA)]$ (middle of REE raw) and to $[Ln(Piv)_3]$ (end of REE raw).

The rare earth metals of the end of the raw form no mixed ligand complexes regardless of the synthesis procedure. To explain this behavior, we performed the quantum-chemical simulation of molecules of the mixed ligand complexes of rare earth metals and studied the composition of the gas phase for lanthanum and lutetium pivalates using mass spectrometry.

QUANTUM-CHEMICAL SIMULATION

The quantum-chemical calculations gave equilibrium geometries of molecules of the homoligand $[Ln(Carb)_3]_n$ (HCarb = HAc, HPiv; n = 1–5) and mixed ligand complexes $[Ln(Piv)_5(MEAH)][MEAH]$, $[Ln(Piv)_3(MEA)]$, and $Ln(Piv)_3(MEA)]_2$, and energy gains of their formation for metals of the beginning (Ln = La), middle (Ln = Eu, Tb), and end of REE raw (Ln = Lu).

Homoligand Lanthanum and Lutetium Carboxylates

Acetates in addition to pivalates were included in a range of objects as models for the calculations of $[Ln(Carb)_3]_n$ (Ln = La, Lu; n = 1–5).

In idealized molecules of $[Ln(Ac)_3]$, the Ln^{3+} cation exists in the trigonal prismatic environment with the coordination number 6. The coordination environment is formed by three bidentate chelate acetate anions (Figs. 3a, 3b). In $[Ln(Ac)_3]$ molecules, the lengths of six Ln–O bonds almost coincide (Table 1). The coordination polyhedron of the Lu^{3+} ion is distorted because of the turn of one base around the axis of the prism by ~20°, which is due to an increase in the electrostatic repulsion of the oxygen atoms of the adjacent anions in the coordination sphere of the smaller Lu^{3+} cation.

According to the quantum-chemical calculation results, lanthanum and lutetium acetates and pivalates are similar in geometry: the coordination environment of the Ln^{3+} cation remains unchanged and the corresponding interatomic distances Ln–O differ less than by 0.01 Å (Table 1). Thus, the presence of bulky *tert*-butyl substituents in the structures of lanthanum and lutetium pivalates does not result in steric hindrances inside the coordination sphere. Therefore, in further calculations of polymerization processes we considered molecules of rare earth metal acetates only.

The analysis of the known structural data [7–15] shows that the rare earth metal carboxylates are characterized by the formation of binuclear fragments in which the rare earth metal ions are bound to each other by bridging and chelate-bridging carboxylate anions.

According to the quantum-chemical calculations, molecules $[La(Ac)_3]_2$ and $[Lu(Ac)_3]_2$ are similar in structure. This structure is typical of the binuclear rare earth metal carboxylates (Fig. 3c). They contain two equivalent rare earth metal cations with the coordination number 7 (the coordination polyhedron is a one-capped trigonal prism) and three pairs of anions with chelate, chelate-bridging, and bridging structural

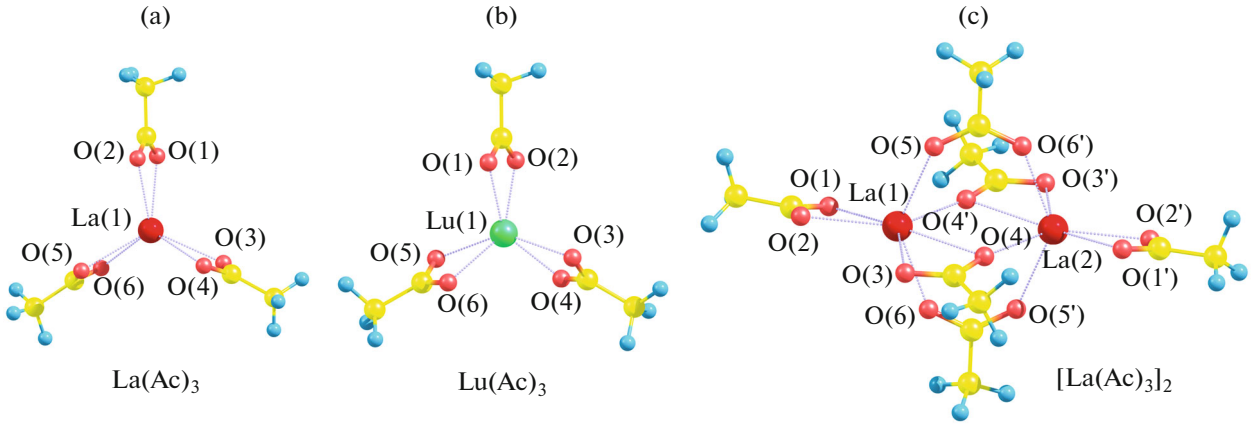

Fig. 3. Optimized geometry of molecules $[Ln(Ac)_3]$ and $[Ln(Ac)_3]_2$.

functions. The Ln–O bond lengths increase over the corresponding distances in $[Ln(Ac)_3]$, and the replacement of the structural function of the carboxyl group O(3)–C–O(4) from the chelate function to chelate-bridging one results in the most increase in the Ln–O(3) and Ln–O(4) distances (Table 1).

The change in the total energy of the system upon dimerization

$$[Ln(Ac)_3] = 1/2[Ln(Ac)_3]_2 \quad (3)$$

($\Delta E_3 = -106$ and -103 kJ/mol for Ln = La and Lu, respectively) indicates that the formation of dimers is energetically favorable. Constant ΔE_3 with a decrease in the ionic radius from La to Lu explains the confrontation of two factors: an increase in the strength of the bridging bonds (Fig. 3c) and the strengthening of the inter-oxygen repulsion. Evidently, in the case of small Ln^{3+} ions of the end of the raw, the chelate-bridging geometry of the carboxyl group is not optimum.

It is established by the results of geometry optimization of the model pentanuclear molecules that the coordination polyhedron of the central La(1) ion is formed by the chelate-bridging acetate anions and represents a three-capped trigonal prism (coordination number 9, Fig. 4a). The coordination polyhedron of the central Lu(1) ion in $[Lu(Ac)_3]_5$ is an octahedron (coordination number 6, Fig. 4b) formed by the oxygen atoms of the bridging acetate anions (average distance Lu–O = 2.23 ± 0.02 Å). A similar coordination mode was observed in the polymer crystal structure $[Tm(Piv)_3]_\infty$ (Fig. 4c) in which the polymer chains are formed only due to the bridging functions of the pivalate anions (average distance Tm–O = 2.176(8) Å) [31].

The change in the total energy (ΔE_{poly}) of the system due to the formation of polymer molecules $[Ln(Ac)_3]_n$ ($n = 5$) can be estimated by the model reaction

$$[Ln(Ac)_3]_4 + Ln(Ac)_3 = [Ln(Ac)_3]_5. \quad (4)$$

Table 1. Interatomic distances Ln–O (Å) in isolated molecules $[Ln(Ac)_3]$, $[Ln(Piv)_3]$, and $[Ln(Ac)_3]_2$ (Ln = La, Lu) according to the quantum-chemical calculation data

Bond	$La(Ac)_3$	$Lu(Ac)_3$	$La(Piv)_3$	$Lu(Piv)_3$	$[La(Ac)_3]_2$	$[Lu(Ac)_3]_2$
Ln–O(1)	2.486	2.285	2.488	2.283	2.535	2.327
Ln–O(2)	2.493	2.277	2.486	2.276	2.505	2.293
Ln–O(3)	2.485	2.280	2.480	2.274	2.553	2.351
Ln–O(4)	2.495	2.281	2.495	2.284	2.760	2.495
Ln–O(5)	2.495	2.280	2.494	2.285	2.444	2.249
Ln–O(6)	2.484	2.282	2.482	2.275	2.453	2.250
Ln–O(4')					2.468	2.255

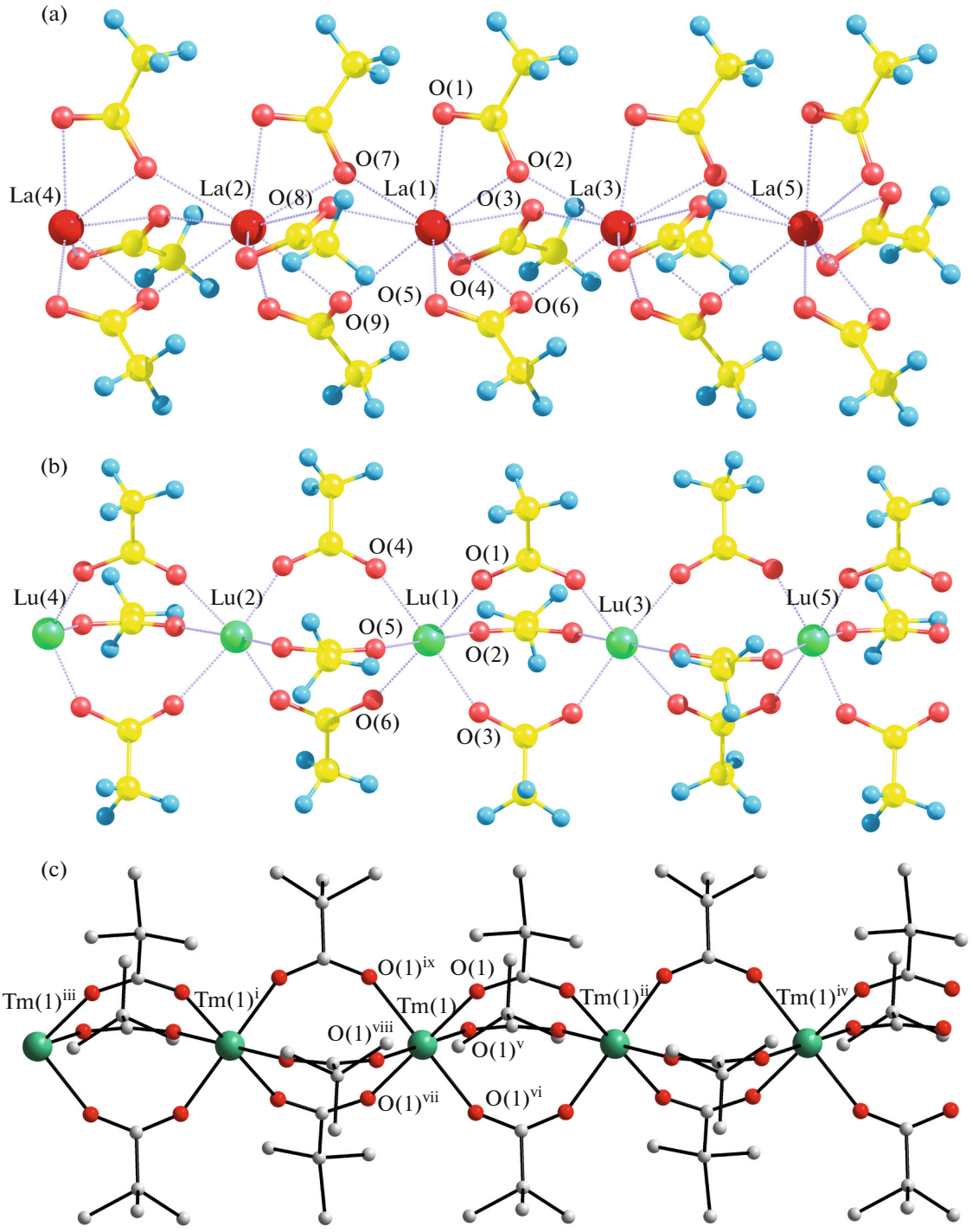

Fig. 4. Optimized geometry of molecules (a) $[La(Ac)_3]_5$ and (b) $[Lu(Ac)_3]_5$ simulating the structure of polymer rare earth metal carboxylates and (c) the fragment of the crystal structure of $[Tm(Piv)_3]_\infty$ [31].

Owing to the chain structure of molecules $[Ln(Ac)_3]_n$, at $n \geq 5$ the coordination environment of the "internal" rare earth metal cations (Ln(1)–Ln(3)) (Figs. 4a, 4b) remains almost unchanged with an increase in n. This makes it possible to consider the change in the energy of the system (ΔE_4) due to reaction (4) to be equal to a change in the energy of the system due to polymerization per Ln atom ($\Delta E_{poly} = \Delta E_4$). The values of ΔE_{poly} were −167 and −245 kJ/mol for $[La(Ac)_3]_\infty$ and $[Lu(Ac)_3]_\infty$, respectively; i.e., the for-

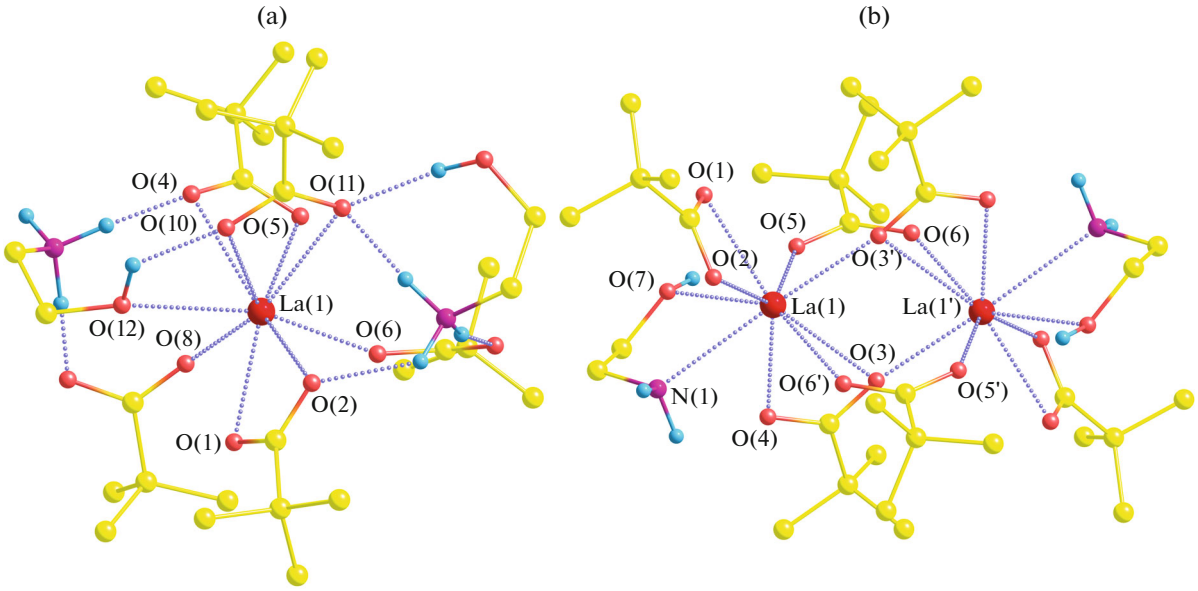

Fig. 5. Optimized geometry of molecules (a) $[Ln(Piv)_5(MEAH)][MEAH]$ and (b) $[La(Piv)_3(MEA)]_2$; Ln = La, Eu, Tb, and Lu (some hydrogen atoms are omitted).

mation of polymer chains is energetically more favorable than the formation of dimeric molecules ($|\Delta E_{poly}| > |\Delta E_3|$). The stability of polymeric carboxylates increases in the raw of rare earth metals.

Mixed Ligand Rare Earth Metal Carboxylates with Monoethanolamine

Quantum-chemical simulation was performed for the addition products of neutral MEA and two ion pairs to La, Eu, Tb, and Lu pivalates: $[Ln(Piv)_3(MEA)]$ and $[Ln(Piv)_5(MEAH)][MEAH]$, respectively.

The calculations show that in molecule $[Ln(Piv)_5(MEAH)][MEAH]$ (Ln = La, Eu, and Tb) the rare earth metal cation with the coordination number 9 coordinates three bidentate chelate and two monodentate terminal pivalate anions, as well as one oxygen atom of the $MEAH^+$ cation (Fig. 5a). In molecule $[Lu(Piv)_5(MEAH)][MEAH]$ the lutetium cation has the coordination number 8 and coordinates only three bidentate chelate and two monodentate terminal pivalate anions.

The main structural motif of molecules $[Ln(Piv)_5(MEAH)][MEAH]$ is retained on going from La to Lu, but the bond lengths with the oxygen atoms of the pivalate anions O(1)–O(11) shorten (Table 2). The length of the Ln–O(12) bond with the oxygen atom of the $MEAH^+$ cation changes nonmonotonically: decreases on going from La to Eu and then increases from Eu to Tb and Lu. This indicates steric hindrances for the rare earth metals of the yttrium subgroup when forming molecules $[Ln(Piv)_5(MEAH)][MEAH]$.

The structures of model molecules $[Ln(Piv)_5(MEAH)][MEAH]$ are fairly well consistent with the data on the crystal structure of $[Ce(Piv)_5(MEAH)][MEAH]$ (Table 2). The most differences in the interatomic Ln–O distances are observed for the O(11) and O(12) atoms and are related to the fact that in the crystal structure of $[Ce(Piv)_5(MEAH)][MEAH]$ they participate in inter-

Table 2. Interatomic distances (Å) in the calculated molecules $[Ln(Piv)_5(MEAH)][MEAH]$ (Ln = La, Eu, Tb, and Lu) and in the crystal structure of $[Ce(Piv)_5(MEAH)][MEAH]$

Bond	La	Eu	Tb	Lu	Ce
Ln–O(1)	2.586	2.477	2.442	2.348	2.547(2)
Ln–O(2)	2.679	2.580	2.560	2.480	2.558(2)
Ln–O(4)	2.688	2.598	2.572	2.524	2.562(2)
Ln–O(5)	2.627	2.522	2.496	2.397	2.607(2)
Ln–O(6)	2.414	2.318	2.295	2.224	2.394(2)
Ln–O(8)	2.462	2.364	2.335	2.202	2.369(2)
Ln–O(10)	2.623	2.539	2.520	2.430	2.566(2)
Ln–O(11)	2.864	2.766	2.719	2.514	2.551(2)
Ln–O(12)	2.766	2.718	2.740	3.827	2.568(2)

Table 3. Interatomic distances Ln–O (Å) in molecules $[Ln(Piv)_3(MEA)]_2$ (Ln = La, Eu, Tb, and Lu)

Bond	$[Ln(Piv)_3(MEA)]_2$			
	La	Eu	Tb	Lu
Ln(1)–O(1)	2.617	2.528	2.506	2.448
Ln(1)–O(2)	2.573	2.471	2.438	2.356
Ln(1)–O(3)	2.911			
Ln(1)–O(4)	2.620	2.509	2.473	2.390
Ln(1)–O(5)	2.542	2.423	2.393	2.317
Ln(1)–O(7)	2.504	2.570	2.539	2.467
Ln(1)–N(1)	2.483	2.653	2.623	2.548
Ln(1)–O(3')	2.664	2.358	2.317	2.234
Ln(1)–O(6')	2.773	2.403	2.374	2.295

molecular hydrogen bonds, whereas they form intramolecular bonds in the calculated isolated molecules (Fig. 5a).

Since rare earth metal carboxylates, including mixed ligand complexes, are characterized by the formation of binuclear molecules, the calculations of the mixed ligand complexes were performed for binuclear $[Ln(Piv)_3(MEA)]_2$ (Ln = La, Eu, Tb, and Lu) and mononuclear $[Ln(Piv)_3(MEA)]$, and the results were used for the estimation of the dimerization energy.

In the centrosymmetric molecule $[La(Piv)_3(MEA)]_2$, the La^{3+} cation (coordination number 9) coordinates the chelate bidentate (O(1), O(2)), chelate-bridging tridentate (O(3), O(4), O(3')), and bridging bidentate (O(5), O(6')) pivalate anions, as well as chelate bidentate (O(7), N(1)) neutral MEA (Fig. 5b, Table 3). When moving along the raw of rare earth metals (using Eu, Tb, and Lu as examples), the chelate-bridging function of the O(3)–C–O(4) ligand is transformed into the chelate function and the coordination number of the central ion becomes equal to 8 (Fig. 5b, Table 3). This induces a sharp increase in the $Ln–O_{MEA}$ and Ln–N(1) bond lengths on going from La to Eu, whereas they regularly decrease in the raw Eu–Lu.

When estimating the energies of mixed ligand complex formation, we took into account the possibility of reactions (5)–(8) to occur and also competitive reaction (4) of the formation of polymer molecules $[Ln(Piv)_3]_n$. The values of ΔE for all considered reactions are summarized in Fig. 6.

$$[Ln(Piv)_3] + 2[MEAH]^+[Piv]^- = [Ln(Piv)_5(MEAH)][MEAH], \quad (5)$$

$$[Ln(Piv)_3] + MEA = [Ln(Piv)_3(MEA)], \quad (6)$$

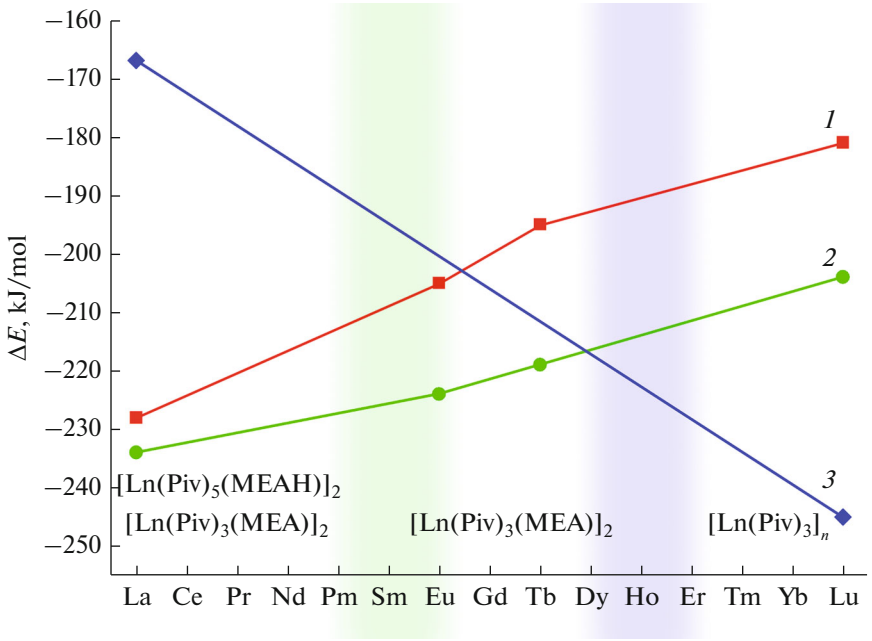

Fig. 6. Changes in the total energy of the system (ΔE) in the course of the competitive reactions forming (*1*) $[Ln(Piv)_5(MEAH)][MEAH]$, (*2*) $[Ln(Piv)_3(MEA)]_2$, and (*3*) $[La(Piv)_3]_n$ for various rare earth metals. The negative value of ΔE corresponds to the energetically favorable process. Vertical lines correspond to boundaries of the stability regions of the molecules of the composition indicated in the figure.

$$[Ln(Piv)_3(MEA)] = 1/2[Ln(Piv)_3(MEA)]_2, \quad (7)$$

$$Ln(Piv)_3 + MEA = 1/2[Ln(Piv)_3(MEA)]_2. \quad (8)$$

According to the calculations (Fig. 6), the formation of $[Ln(Piv)_5(MEAH)_2]$, $[Ln(Piv)_3(MEA)]$, and $[Ln(Piv)_3(MEA)]_2$ from molecules $Ln(Piv)_3$ is energetically favorable for all considered rare earth metals. Noticeably higher energy gains for the formation of mononuclear molecules $[Ln(Piv)_5(MEAH)_2]$ compared to mononuclear $[Ln(Piv)_3(MEA)]$ are due to additional intramolecular hydrogen bonds in molecule $[Ln(Piv)_5(MEAH)][MEAH]$. At the same time, the energy is additionally decreases by 58–80 kJ/mol, and the most stable mixed ligand complexes $[Ln(Piv)_3(MEA)]_2$ are formed due to the dimerization of molecule $[Ln(Piv)_3(MEA)]$ (reaction (7)) (Fig. 6).

The thermodynamic stability of $[Ln(Piv)_5(MEAH)][MEAH]$, $[Ln(Piv)_3(MEA)]_2$, and $[Ln(Piv)_3]_n$ changes in different directions as the radius of the central ion decreases. The values of ΔE for the formation of $[Ln(Piv)_5(MEAH)][MEAH]$ and $[Ln(Piv)_3(MEA)]_2$ increase from La to Lu with different rates, whereas they decrease, on the contrary, for $[Ln(Piv)_3]_n$. This is quite expected, because a high coordination number of 9 (in molecules of the mixed ligand complexes) is not characteristic of rare earth metals of the end of the raw. As a result, restricted regions of stability can be distinguished for these compounds in the raw of the rare earth metals. For example, $[Ln(Piv)_5(MEAH)][MEAH]$ and $[Ln(Piv)_3(MEA)]_2$ are most stable from La to Eu (ΔE_5 and ΔE_8 differ less than by 20 kJ/mol). The stability of $[Ln(Piv)_3(MEA)]_2$ predominated in the region from Gd to Er. Finally, compounds $[Ln(Piv)_3]_n$ demonstrate the highest stability for metals of the end of the raw from Tm to Lu.

In spite of the conventional character of the presented estimates, the regularities revealed from the calculations are completely consistent with the experimental results (Fig. 6, Scheme 2).

MASS SPECTROMETRIC STUDY OF LANTHANUM AND LUTETIUM *tris*-PIVALATES

The compositions of the gas phases over $[La(Piv)_3]_\infty$ and $[Lu(Piv)_3]_\infty$ were studied in temperature ranges of 533–643 and 580–690 K, respectively. In the mass spectra of the gas phase over both substances (see Experimental), the ionic current $I[La_2(Piv)_5]^+$ corresponds to the most intense lines. A saturated vapor over compounds $[La(Piv)_3]_\infty$ and $[Lu(Piv)_3]_\infty$ consists of dimeric molecules $[Ln_2(Piv)_6]$. The saturated vapor pressure and the enthalpy of sublimation of the dimeric molecules via reactions (9) and (10) were calculated from the results of full isothermal evaporation [32] and the temperature dependences of the ionic current intensities for $[La_2(Piv)_5]^+$, $[La_2(Piv)_4]^+$, $[La_2(Piv)_3]^+$ and $[Lu_2(Piv)_5]^+$, $[Lu(Piv)_2OH]^+$, $[Lu_2(Piv)_2 - 3CH_3]^+$

$$2\,[La(Piv)_3]_s = [La_2(Piv)_6]_g, \quad (9)$$

$$\Delta_s H^o(La(Piv)_3, s) = 208.7 \pm 16.3 \text{ kJ/mol}$$
$$(530 \le T \le 636 \text{ K}),$$

$$P(La_2(Ppiv)_6, 590 \text{ K}) = 3.1 \times 10^{-1} \text{ Pa};$$

$$2\,[Lu(Piv)_3]_s = [Lu_2(Piv)_6]_g, \quad (10)$$

$$\Delta_s H^o(Lu(Piv)_3, s) = 230.1 \pm 16.3 \text{ kJ/mol}$$
$$(580 \le T \le 683 \text{ K}),$$

$$P(Lu_2(Piv)_6, 673 \text{ K}) = 9.8 \times 10^{-2} \text{ Pa}.$$

The values obtained for the enthalpies of sublimation of lanthanum and lutetium pivalates in the form of molecules $[Ln_2(Piv)_6]$ agree with the earlier obtained data for dimeric molecules of samarium (211.7 ± 9.5 kJ/mol) [33], europium (209.5 ± 11.2 kJ/mol) [34], and thulium (228.8 ± 3.6 kJ/mol) pivalates [31]. The enthalpies of sublimation of $[Nd(Piv)_3]_s$ and $[Er(Piv)_3]_s$, being 205 and 219 kJ/mol, respectively, were also estimated from the temperature dependence of the saturated vapor pressure using published data [35].

Thus, the enthalpy of sublimation of rare earth metal pivalates increases on going from La to Lu, which is due to polymer chains in their structures, the strength of which increases with a decrease in the ionic radius of the rare earth metal. This distinguishes volatile polymer pivalates from the widely known volatile rare earth metal dipivaloylmethanates in which intermolecular interactions weaken in the raw of rare earth metals, resulting in an increase in volatility (Fig. 7).

Note that monomeric molecules $[Sm(Piv)_3]$ were observed along with dimeric molecules $[Sm_2(Piv)_6]$ over samarium pivalate. The enthalpy of sublimation of $[Sm(Piv)_3]$ was 189.2 ± 11.3 kJ/mol [33]. The obtained data make it possible to calculate the enthalpy of dissociation of the dimer in gas-phase reaction (11)

$$1/2[Sm_2(Piv)_6]_g = [Sm(Piv)_3]_g \quad (11),$$

which is equal to 83.3 ± 9.3 kJ/mol and is well consistent with ΔE_3 for Ln = La (106 kJ/mol) theoretically calculated from backward reaction (3).

Thus, the data of mass spectrometry form a single pattern with the results of synthesis and quantum-chemical calculations. The enhanced strength of the polymer chains of pivalates of the rare earth metals of

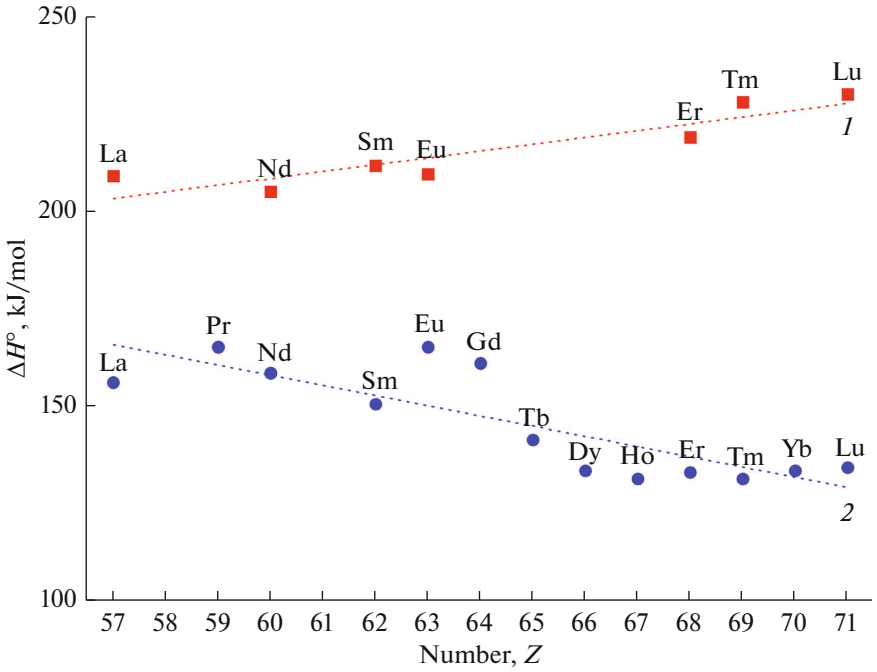

Fig. 7. Change in the sublimation enthalpy of (*1*) pivalates and (*2*) and dipivaloyl methanates along the raw of the rare earth metals [36, 37].

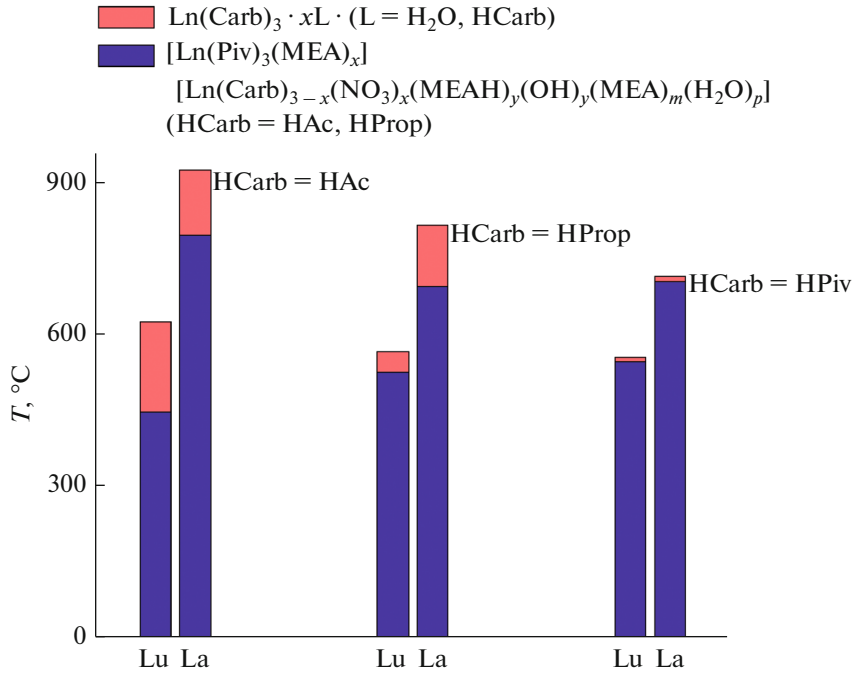

Fig. 8. Diagram of changing the final decomposition temperatures for the rare earth metals carboxylates and their mixed ligand complexes with MEA in air.

the end of the raw leads to a decrease in volatility in the raw of rare earth metal pivalates and to the formation of homoligand pivalates in the system with monoethanolamine instead of mixed ligand complexes as it takes place for the rare earth metals of the beginning of the raw.

THERMAL STABILITY OF THE MIXED LIGAND CARBOXYLATE COMPLEXES OF RARE EARTH METALS WITH MEA AND THEIR USE FOR THE PREPARATION OF OXIDE MATERIALS

To evaluate prospects of the synthesized mixed ligand complexes of rare earth metal carboxylates with MEA as metal-organic precursors for the MOCSD method, we studied their thermal stability in air and compared with that for $Ln(Carb)_3 \cdot nH_2O$ (HCarb = HAc, HProp, and HPiv) (Fig. 8) [21].

The thermal behavior in air of rare earth metal acetates, propionates, and pivalates is similar [3–8, 25]. Their transformation into the corresponding oxides is a multistep process proceeding through the step of oxocarbonate formation, which is distinctly seen in the thermal gravimetric (TG) curves. As a whole, the temperature of oxide formation from rare earth metal carboxylates decreases in the raw of rare earth metals and on going from $[Ln(Ac)_3]$ to $[Ln(Piv)_3]$ from ~900 to 700°C. Cerium carboxylates completely decompose in a range of 400–450°C, which is related to the oxidation of Ce^{3+} to Ce^{4+}.

The thermal analysis showed that the mixed ligand hydroxo complexes $[Ln(Carb)_{3-x-y}(NO_3)_x(OH)_y(MEA)_w(H_2O)_z]$ (HCarb = HAc and HProp) decomposed to the corresponding oxides at the temperatures lower (by 50–180°C) than the corresponding $Ln(Carb)_3$ did (Fig. 8). Mixed ligand complexes $[Ln(Piv)_3(MEA)]$ eliminate MEA in a range of 150–300°C and then decompose in the same way as the initial pivalates.

Based on the thermal analysis data, we can suggest that mixed ligand rare earth metal hydroxoacetates and hydroxopropionates with MEA decomposing to oxides at lower temperatures are most interesting and promising as MOP [38]. The efficiency of these precursors was demonstrated for the deposition of biaxially textured CeO_2 films [20].

The metal-organic precursor $\{Ce(NO_3)_3 \cdot 6H_2O$ + 3HAc + MEA-diglyme$\}$ was synthesized for the preparation of the oxide CeO_2 coating. Deposition was carried out on the Ni-containing tape served as a substrate under the optimal conditions established earlier [20]. The surface of the obtained oxide coating has no defects and is formed of spherical aggregates ~0.3 μm in size (Fig. 9). The texture and morphology of the

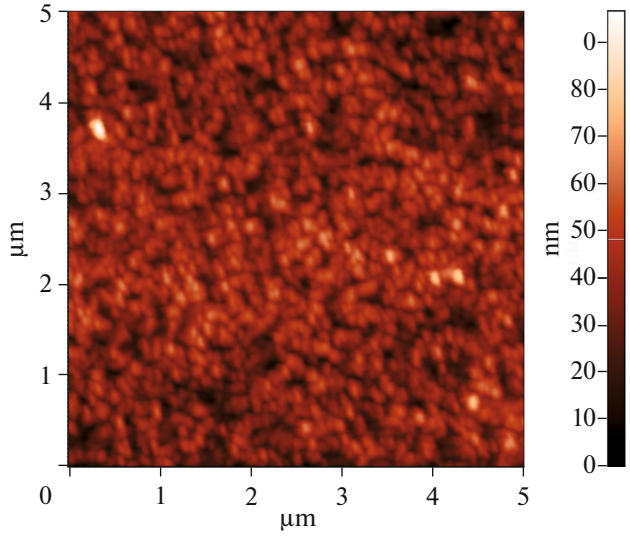

Fig. 9. Morphology of the CeO_2 film surface according to the data of atomic force microscopy on a surface area of 5×5 μm^2 [20].

CeO_2 film corresponds completely to the requirements imposed on buffer layers in heterostructures of high temperature superconducting wires of the second generation.

Thus, specific features of the reaction with MEA and the main differences in non-aqueous media were revealed for acetates, propionates, and pivalates of rare earth metals of the cerium and yttrium groups. The nature of the carboxylate ligand and rare earth ion and the synthesis conditions are the main factors affecting the composition of the synthesized product. The gel-like mixed ligand hydroxo complexes $[Ln(Carb)_{3-x-y}(NO_3)_x(OH)_y(MEA)_w(H_2O)_z]$ are formed in the case of rare earth metal acetates and propionates regardless of the synthesis method, whereas the formation of several products, viz., $[Ln(Piv)_5(MEAH)][MEAH]$, $[Ln(Piv)_3(MEA)]$, or $[Ln(Piv)_3]$, is possible for pivalates. Quantum-chemical simulation was used to interpret specific features of the formation of the mixed ligand complexes of rare earth metal pivalates with MEA. The composition of the synthesis product was shown to be determined by the nature of the rare earth metal: the formation of $[Ln(Piv)_5(MEAH)][MEAH]$ and/or $[Ln(Piv)_3(MEA)]$ is characteristic of the beginning of the raw, only $[Ln(Piv)_3(MEA)]$ is characteristic of the middle of the raw, and mixed ligand complex formation does not occur at all for rare earth metals of the end of the raw. An increase in the stability of pivalates in the raw of rare earth metals was also confirmed by the data of mass spectrometry. The thermal analysis of the synthesized mixed ligand complexes showed that the mixed ligand hydroxo complexes $[Ln(Carb)_{3-x-y}$-

Table 4. Most intense ions in the ESI-MS spectra of MEA and ion pairs $[MEAH]^+[Carb]^-$ in *iso*-PrOH

Composition of solution	Major ions (*m/z*)
MEA	$[Na(MEA)_3]^+$ (206.2/206.2); $[(MEAH)^+(MEA)_3]^+$ (244.2/245.3); $[Na(MEA)(H_2O)]^+$ (102.3/103.0); $[Na_2(MEA\text{-}H)(MEA)_3]^+$ (289.2/289.3); $[MEAH]^+$(62.4/62.0)
Hac–MEA	$[(MEAH)_2(Hac)_3]^{2+}$ (152/152.17); $[Na_2(Ac)(MEA)]$ (166.0/166.1); $[Na(MEA)_2]$ (145.0/145.2); $[MEAH]^+$(62.4/62.0)
HProp–MEA	$[Na_2(Prop)_2(MEAH)(HProp)_2]^{2+}$ (201/201.2); $[Na(MEA)(H_2O)]^+$ (102.3/103.0); $[MEAH]^+$ (62.4/62.0)
Hpiv–MEA	$[(HPiv)(MEAH)(H_2O)_2]^+$ (201.5/200.26); $[(HPiv)(MEAH)]^+$ (163.4/164.2); $[MEAH]^+$(62.4/62.0)

$(NO_3)_x(OH)_y(MEA)_w(H_2O)_z]$ (HCarb = HAc, HProp) decomposed to oxides at the temperatures lower than those of the initial carboxylates or mixed ligand complexes $[Ln(Piv)_5(MEAH)][MEAH]$ and $[Ln(Piv)_3(MEA)]$. Metal-organic precursors $[Ce(Carb)_{n-x-y}(NO_3)_x(OH)_y(MEA)_w(H_2O)_z]$ are of special interest, since they are highly soluble in organic solvents and easily decompose in air to form oxide in a range of 350–400°C.

EXPERIMENTAL

Elemental analyses of the compounds were carried out on a Vario Micro Cube C, H, N analyzer (Elementar, Germany) at the Chair of Organic Chemistry of the Department of Chemistry at the Moscow State University. Analyses to rare earth metals were carried out by complexonometric titration. The IR spectra of the complexes were recorded on a FTIR Spectrum One instrument (PerkinElmer) in the attenuated total internal reflection mode in a range of 400–4000 cm^{-1}.

Synthesis of $[MEAH^+][Piv^-]$. Monoethanolamine (4 mmol) was added to a solution of HPiv (4 mmol) in CH_3CN (5 mL), the mixture was stirred for 2 h, and the solvent was slowly evaporated. The yield of a white crystalline precipitate of $[MEAH^+][Piv^-]$ was 0.62 g (95%).

For $C_7H_{17}NO_3$

anal. calcd., %:	C, 51.5;	H, 10.4;	N, 8.6.
Found, %:	C, 51.5;	H, 10.2;	N, 8.6.

IR, ν, cm^{-1}: 3305, 2956, 2904, 2871, 1649, 1619, 1507, 1487, 1458, 1407, 1361, 1306, 1278, 1226, 1180, 1130, 1068, 1032, 938, 887, 838, 796, 593. ^1H NMR ($CDCl_3$), δ, ppm: 1.19 (s, 9H), 2.99 (tr, 2H), 3.76 (tr, 2H), 6.65 (s, 6H).

Synthesis of the mixed ligand complexes. The initial $Ln(Piv)_3$ (Ln = La, Eu, Gd, Tb, Dy, Y, Er, Tm, Yb, and Lu) were synthesized using a known procedure [12]. According to a described procedure [21], a solution of $Ln(NO_3)_3 \cdot 6H_2O$ (1 mmol) in CH_3CN (20 mL) was added to a solution of $[MEAH^+][Piv^-]$ (5 mmol) in CH_3CN (100 mL) followed by stirring for 2 h without heating. Finely crystalline precipitates of the mixed ligand complexes $[La(Piv)_3(MEA)]$ (type **I**) (Ln = La, Eu, Gd, Tb, Dy, Y, Ho, and Er) and $Ln(Piv)_3$ (Ln = Tm, Yb, and Lu) (yield ~0.4 g). Precipitates of the mixed ligand complexes $[Ln(Piv)_5(MEAH)][MEAH]$ (Ln = La, Eu, and Gd), $[La(Piv)_3(MEA)]$ (type **II**) (Ln = Tb, Dy, Y, Ho, and Er), and $Ln(Piv)_3$ (Ln = Tm, Yb, and Lu) were obtained similarly but using the corresponding $Ln(Piv)_3$ as the initial compounds. The identity of the compositions of the obtained products to the ascribed formulas was established by all results of elemental, IR, and X-ray phase analysis and literature data [12, 21, 22].

The ESI-MS analysis of solutions in organic solvents was carried out on an Agilent LCMSD 1100 SL instrument with sample ionization under atmospheric pressure in the positive ion detection mode using a mass analyzer of the ion trap type (Table 4). Conditions of spectra recording were as follows: the flow rate of the solution was 10 μL/min, the temperature of the drying gas (N_2) was 120–320°C, the voltage on the nebulizer was 3.5–6.0 kV, and the voltage on the capillary was varied from 0 to 220 V. The values of *m/z* and isotopic distribution (^{151}Eu, ^{153}Eu; ^{140}Ce, ^{142}Ce) were calculated using the IsoPro program.

^1H NMR spectra were recorded on a Bruker Avance-400 instrument (400 MHz; $CDCl_3$, CD_3CN/TMS).

X-ray phase analyses of powders were carried out on a Rigaku SmartLab diffractometer (CuK_α, graphite

Table 5. Crystallographic parameters for the mixed ligand complexes $[Ln(Piv)_5(MEAH)][MEAH]$ (Ln = La, Ce, Eu, and Gd)

Parameter	$[Ln(Piv)_5(MEAH)][MEAH]$			
	La	Ce [22]	Eu	Gd
T, K	300	100	300	300
Space group	$P2_1/n$	$P2_1/n$	$P2_1/n$	$P2_1/n$
Z	4	4	4	4
a, Å	15.427(5)	15.3743(16)	15.347(5)	15.340(5)
b, Å	11.537(4)	11.4614(12)	11.505(4)	11.505(5)
c, Å	23.570(7)	22.985(2)	23.245(6)	23.229(7)
β, deg	105.267(19)	105.515(2)	105.37(2)	105.50(2)
V, Å^3	4047.0(12)	3902.6(7)	3957.3(12)	3950.7(16)
FOM	$F_{29} = 47$	$R_1 = 0.0394$ $\omega R_2 = 0.0966$	$F_{27} = 43$	$F_{26} = 32$

Table 6. Mass spectra of the saturated vapor over $[La(Piv)_3]_\infty$ and $[Lu(Piv)_3]_\infty$ ($U_{ionization}$ = 70 V)

$[La(Piv)_3]_\infty$ (T = 593 K)		$[Lu(Piv)_3]_\infty$ (T = 672 K)	
Ion	Ionic current, %	Ion	Ionic current, %
$[La(Piv)OH]^+$	29	$[Lu(Piv)]^+$	8
$[La(Piv)OOC]^+$	9	$[Lu(Piv)_2OH]^+$	65
$[La(Piv)_2 - CH_3]^+$	17	$[Lu_2(Piv)_2 - 3CH_3]^+$	21
$[La(Piv)_2OH]^+$	43	$[Lu_2(Piv)_2CO]^+$	11
$[La_2(Piv)OCC]^+$	16	$[Lu_2(Piv)_3]^+$	9
$[La_2(Piv)_2 - CH_3]^+$	34	$[Lu_2(Piv)_3OH]^+$	4.5
$[La_2(Piv)_3OCC]^+$	14	$[Lu_2(Piv)_5 - CH_3]^+$	3
$[La_2(Piv)_3]^+$	26	$[Lu_2(Piv)_5]^+$	100
$[La_2(Piv)_4]^+$	65		
$[La_2(Piv)_5]^+$	100		

monochromator, λ = 1.54187 Å) in the Bragg–Brentano geometry (2θ = 5°–60°). The X-ray diffraction patterns of all compounds were indexed. The unit cell parameters for the mixed ligand complex $[Ln(Piv)_5(MEAH)][MEAH]$ are presented in Table 5.

Thermal analysis was carried out on Derivatograph Q1500D and NETZSCH (Germany, series STA 409) instruments in a temperature range of 20–1000°C in air or in an argon flow (weighed sample 40–50 mg, heating rate 10 K/min, alundum crucible).

X-ray diffraction analyses were carried out on a Bruker SMART APEX2 CCD diffractometer (MoK_α, graphite monochromator, λ = 0.71072 Å) at 100 K. Single crystals of $[MEAH^+][Piv^-]$ suitable for analysis were obtained by the slow crystallization of a solution in $CDCl_3$ in an NMR tube at 5°C. All calculations were performed using the SHELXTL PLUS 5.0 program package [39]. The structure was solved by direct methods and refined by full-matrix least squares with anisotropic thermal parameters for all non-hydrogen atoms. The hydrogen atoms of the OH, and NH_3^+ groups were localized from the difference Fourier syntheses and refined in the riding model. The positions of other hydrogen atoms were calculated geometrically and refined in the riding model with fixed isotropic thermal parameters. The full array of crystallographic data for the structure of $[MEAH^+][Piv^-]$ was deposited at the Cambridge Crystallographic Data Centre (CCDC file 867336; deposit@ccdc.cam.ac.uk; http://www.ccdc.cam.ac. uk/data_request/cif).

Quantum-chemical simulation of the rare earth metal carboxylates was performed for isolated molecules in the FireFly 8.1 program package [40] in the framework of the electron density functional theory

(B3LYP functional) using the 6-31G* basis sets for C, O, N, and H atoms and the quasi-relativistic Stuttgart–Cologne effective core potentials with a large core (ECP46MWB, ECP52MWB, ECP54MWB, and ECP60MWB) with the corresponding basis sets for La, Eu, Tb, and Lu [41, 42]. The geometry of molecules was optimized without symmetry restraints.

The change in the total energy of the system (ΔE_i) due to the occurrence of model reactions (3)–(8) was calculated by the equations

$$\Delta E_3 = ½[Ln(Ac)_3]_2 - [Ln(Ac)_3],$$

$$\Delta E_{poly} = \Delta E_4 = E[Ln(Ac)_3]_5 - E[Ln(Ac)_3]_4 - E[Ln(Ac)_3],$$

$$\Delta E_5 = E[Ln(Piv)_5(MEAH)][MEAH] - 2E[MEAH]^+[Piv]^- - E[Ln(Piv)_3],$$

$$\Delta E_6 = E[Ln(Piv)_3(MEA)] - E[MEA] - E[Ln(Piv)_3],$$

$$\Delta E_7 = ½(E[Ln(Piv)_3(MEA)]_2 - 2E[Ln(Piv)_3(MEA)]),$$

$$\Delta E_8 = \Delta E_6 + \Delta E_7.$$

Here E are the total energies of the indicated molecules.

Mass spectral analysis of the gas phase. The vaporization of $[La(Piv)_3]_\infty$ and $[Lu(Piv)_3]_\infty$ was studied by the effusion Knudsen method with mass spectral analysis of the gas phase on an MS 1301 instrument with an extended range of mass numbers (to 1300 amu, Table 6). Standard molybdenum Knudsen cells with a ratio of the vaporization surface area to the effusion surface area of ~600 were used. The temperature was measured with the Pt/Pt (Rh) thermocouple and was maintained constant with an accuracy of ±1°C.

ACKNOWLEDGMENTS

The authors are grateful to the X-ray Structural Center of the Nesmeyanov Institute of Organoelement Compounds (Russian Academy of Sciences) and personally to Prof. K.A. Lysenko for an opportunity to carry out X-ray diffraction analyses. The quantum-chemical calculations were performed using facilities of the Supercomputing Center of the Moscow State University.

This work was supported by the Russian Foundation for Basic Research, project no. 11-03-01208-a.

REFERENCES

1. Martin, L.W., Chu, Y.-H., and Ramesh, R., *Mater. Sci. Eng., R.*, 2010, vol. 68, p. 165.
2. *Chemical Solution Deposition of Functional Oxide Thin Films,* Schneller, T., Waser, R., Kosec, M., and Payne, D., Eds., Dordrecht: Springer, 2013.
3. Shaplygin, I.S., Komarov, V.P., and Lazarev, V.B., *J. Therm. Anal.*, 1979, vol. 15, p. 215.
4. Mayer, I. and Kassierer, F., *J. Inorg. Nucl. Chem.*, 1966, vol. 28, p. 2430.
5. Patil, K.C., Chandrashekhar, G.V., George, M.V., et al., *Can. J. Chem.*, 1968, vol. 46, p. 257.
6. Arii, T., Kishi, A., Ogawa, M., et al., *Anal. Sci.*, 2001, vol. 17, p. 875.
7. *Gmelin Handbook of Inorganic Chemistry*, Berlin, 1984, Syst No. 39, vol. D5.
8. Junk, P.C., Kepert, C.J., Min, W., et al., *Aust. J. Chem.*, 1999, vol. 52, p. 437.
9. Ouchi, A., *Coord. Chem. Rev.*, 1988, vol. 92, p. 29.
10. Ciontea, L., Nasui, M., Petrisor, T.Jr., et al., *Mater. Res. Bull.*, 2010, vol. 45, p. 1203.
11. Martynova, I.A., Tsymbarenko, D.M., and Kuz'mina, N.P., *Russ. J. Coord. Chem.*, 2014, vol. 40, no. 8, p. 565.
12. Khudyakov, M.Yu., Kuz'mina, N.P., Pisarevskii, A.P., et al., *Russ. J. Coord. Chem.*, 2002, vol. 28, no. 7, p. 521.
13. Dobrokhotova, Zh.V., Fomina, I.G., Aleksandrov, G.G., et al., *Russ. J. Inorg. Chem.*, 2009, vol. 54, no. 5, p. 668.
14. Kiseleva, E.A., Troyanov, S.I., and Korenev, Yu.M., *Russ. J. Coord. Chem.*, 2006, vol. 32, no. 1, p. 57.
15. Porai-Koshits, M.A., *Itogi Nauki Tekh., Ser.: Kristallokhim.*, Moscow: VINITI, 1981.
16. Gharia, K.S., Singh, M., Mathur, S., et al., *Synt. React. Inorg. Met.-Org. Chem.*, 1980, vol. 10, p. 403.
17. Tudor, V., Marin, G., Lloret, F., et al., *Inorg. Chim. Acta*, 2008, vol. 361, p. 3446.
18. Kufelnicki, A., Tomyn, S.V., Nedelkov, R.V., et al., *Inorg. Chim. Acta*, 2010, vol. 363, p. 2996.
19. Yilmaz, V.T., Andac, O., Karadag, A., et al., *J. Mol. Struct.*, 2002, vol. 641, p. 119.
20. Kuz'mina, N.P., Ibragimov, S.A., Makarevich, A.M., et al., *Chem. Mater.*, 2010, vol. 22, p. 5803.
21. Martynova, I.A., Kardashev, S.V., and Kuz'mina, N.P., *Vestn. Mosk. Univ., Ser. 2: Khim.*, 2012, vol. 53, no. 1, p. 24.
22. Kuz'mina, N.P., Martynova, I.A., Tsymbarenko, D.M., et al., *Inorg. Chem. Commun.*, 2011, vol. 14, p. 180.
23. Pinkert, A., Marsh, K.N., and Pang, S., *Ind. Eng. Chem. Res.*, 2010, vol. 49, p. 11809.
24. Temin, S.C., *Org. Chem.*, 1956, vol. 21, p. 250.
25. Kuzmina, N.P., Martynenko, L.I., Zoan T.A., et al., *Neorg. Khim.*, 1994, vol. 39, no. 4, p. 538.
26. Abbas, G., Lan, Y., Kostakis, G., et al., *Inorg. Chim. Acta*, 2008, vol. 361, p. 3494.
27. Reutov, O.A., Kurts, A.L., and Butin, K.P., *Organicheskaya khimiya* (Organic Chemistry), Moscow: Binom. Laboratoriya znanii, 2004, part 3, p. 421.
28. Gutmann, V., *The Donor Acceptor Approach to Molecular Interactions*, New York: Plenum, 1978.
29. Burger, K., *Solvation, Ionic and Complex Formation Reactions in Non-aqueous Solvents*, Budapest: Akadémiai Kiadó, 1983, p. 268.
30. Kharchenko, A.V., Makarevich, A.M., Lysenko, K.A., et al., *Russ. J. Coord. Chem.*, 2010, vol. 36, no. 11, p. 804.
31. Fomina, I., Dobrokhotova, Zh., and Aleksandrov, G., *J. Solid State Chem.*, 2012, vol. 185, p. 49.

32. Sidorov, L.N., Korobov, M.V., and Zhuravleva, L.V., *Mass-spektral'nye termodinamicheskie issledovaniya* (Mass-Spectral Thermodynamic Investigtions), Moscow: Mosk. Univ., 1985.
33. Malkerova, I.P., Alikhanyan, A.S., Fomina, I.G., et al., *Russ. J. Inorg. Chem.*, 2009, vol. 54, no. 5, p. 734.
34. Malkerova, I.P., Alikhanyan, A.S., Fomina, I.G., et al., Russ. J. Inorg. Chem., 2010, vol. 55, no. 1, p. 53.
35. Zoan, T.A., Kuzmina, N.P., Frolovskaya, S.N., et al., *J. Alloys Comp.*, 1995, vol. 225, p. 396.
36. Santos, L.S., *J. Chem. Thermodyn.*, 1997, vol. 29, p. 661.
37. Sicre, J.E., *J. Am. Chem. Soc.*, 1969, vol. 91, no. 13, p. 3476.
38. Martynova, I.A., Tsymbarenko, D.M., Kamenev, A.A., et al., *Izv. Akad. Nauk, Ser. Khim.*, 2013, vol. 62, no. 6, p. 1454.
39. Sheldrick, G.M., *SHELXTL. Version 5.10. Structure Determination Software Suite*, Madison: Bruker AXS, 1998.
40. Granovsky, A.A., *Firefly version* 8, http://classic.chem.msu.su/gran/firefly/index.htm
41. Dolg, M., Stoll, H., Savin, A., et al., *Theor. Chim. Acta*, 1989, vol. 75, p. 173.
42. Dolg, M., Stoll, H., and Preuss, H., *Theor. Chim. Acta*, 1993, vol. 85, p. 441.

Translated by E. Yablonskaya